Dear prof. Fogg,

We are very grateful for your constructive comments to improve the revision of our manuscript. We carefully revised the text by incorporating the comments one by one.

The detailed revision is presented in the response to each comment:

Comment 1. *The authors' response to Comment 2 of Reviewer 1 needs to be reconsidered and reworked because the authors misunderstood what is meant by resistivity log calibration. Because you are using the logged resistivity values quantitatively (e.g., in Archie's law), Reviewer 1 correctly pointed out that to do so requires that the logs have been calibrated. This means that when the logs were run, a geophysical log calibration process should have been done that produces resistivity values that would be consistent enough for one to compare quantitatively the log resistivity values among the different logs. Log calibration is supposed to be done in the field by the person who performs the logging, but in practice, it often is not done and can certainly undermine the validity of Archie's law calculations, among other things. Reviewer 1 also correctly pointed out that salinity of the formation water strongly affects log resistivity, and that too should be taken into account. I do not see any sign that you addressed that.*

I suspect that you do not know whether the logs were calibrated, and that it is unlikely that you would be able to acquire such information any time soon. Nevertheless, you need to figure out how to modify the manuscript to deal with the log calibration issue. One approach might be to acknowledge that you cannot verify whether the logs were calibrated, and then point out that this presents another source of error that could be reduced in future studies by only using logs that have been calibrated. In essence, you would be working under the assumption that the logs have been calibrated in order to present your work as a proof of concept.

Response: Thank you for the clarification of Comment 2 by Reviewer 1. Yes, we don't know and we cannot verify whether the logs were calibrated or not in the field and how the salinity of the formation water has been accounted for. Following your suggestion, we explicitly acknowledged this lack of information (lines 140-146) and pointed out this might be another source of uncertainty that can be reduced in our future studies (lines 385-386).

You also need to deal with the issue of groundwater quality (TDS) and it's effects on the resistivity values by either explaining that TDS variations laterally or vertically in the aquifer system are minimal (which seems unlikely) or that this is just another limiting assumption that could be eliminated by performing more complete analyses in the future.

Response: The pore fluid conductivity was estimated by using total dissolved solids (TDS) and temperature data. Lateral and vertical TDS variations in the aquifer system impact on the measured resistivity values. We focused on the resistivity data below water table. Because of the relatively limited dataset and the observed small variability in the TDS, in this paper we ignored the TDS variations in the vertical direction (Line 167-170). In discussion section, we have pointed out that a more complete investigation on the TDS (salinity) distribution in the whole fan will be carried out in the future to improve the reliability of our analyses (lines 382-383).

Comment 2*. The authors' response to Reviewer 3 needs some more modification to reflect deeper introspection about their work. I agree that the tone of Reviewer 3's criticisms is somewhat harsh, and from the point of view of an author, can be quite off-putting. There are, however, some important kernels of truth in several of Reviewer 3's comments that are worthy of more careful consideration. In particular, your response to Reviewer 3's Comment 1 needs some reconsideration, given that your assertion of the novelty of the work is based on the incorporation of resistivity logs (see my point 1 above with respect to Reviewer 1). I think that your assertion that the novelty stems from incorporation of the resistivity logs quantitatively into the work may be OK, but here again, you need the caveat(s) regarding how quantitatively representative the logs actually are.*

Response: Yes, we believe that the third reviewer also gave us some valuable comments and we address them along with those from Reviewer 1. In our responses to the comments of Reviewer 1 we pointed out that in this study we assumed the logs have been calibrated, which might be another source of uncertainty that can be reduced in future studies.

Your response to Reviewer 3's statement: "(1) there is no directional non-stationarity (e.g. no radial variability of the depositional major axis; no stratigraphic dip),…" seems incomplete, and I am not sure you fully understood it. Reviewer 3's statement (1) above is basically asking why you did not model the spatial variations in the strike and dip of the fan facies. I am not finding an answer to that question in your responses to either Reviewer 1 (whom you refer to in this context) or to Reviewer 3. It appears to me that you did not have information on variations in dip or strike orientations of the variogram structure, which is why you did not account for that. This sort of thing should be included in the part of your paper that discusses model limitations and how it might be improved in the future.

Response: In our previous response we stated that they were the same comments provided by Reviewer #1 in "General comments" #6. The reviewer could refer to the responses provided to Reviewer #1. Now we added more clarification to these comments as the editor suggested. We have used available information along the dip direction, see Figure 7. In the description of Figure 9, we added a sentence to indicate that "since we simulate the dip direction along the main water flow direction and the strike-directional semivariogram is assumed to be similar as that in dip direction (due to lack of enough data to estimate the parameters for the strike-directional semivariogram), the simulated facies in the fan apex do not show a radiating pattern. More information about simulating the radiating pattern can be found from Carle and Fogg (1997) and Fogg et al. (1998)" (Line 330-334).

The estimated range and variance for the semivariograms of dip direction in Zone 2 and Zone 3 were given in Table 4 and Fig. 7. Accurate descriptions of the semivarigrams in the dip and lateral directions will be included in our future study to improve the developed three-dimensional permeability field (Line 383-385).

The list of all relevant changes made in the manuscript was as follows.

1) We added some sentences (Line 140-146) on logs calibration according to the editor's suggestion.
2) Detail information on simulating the stochastic faices were given from Line 266 to 270.
3) We added more clarification on semivariogram (Line 330-332) as the editor suggested.
4) We pointed out the things to do in our future study to improve the developed three-dimensional permeability field (Line 383-386).

Modelling 3D permeability distribution in alluvial fans using facies architecture and geophysical acquisitions

Lin Zhu [1], Huili Gong [1], Zhenxue Dai [2,3], Gaoxuan Guo [4], Pietro Teatini [5]

[1]College of Resource Environment and Tourism, Capital Normal University, Laboratory Cultivation Base of Environment Process and Digital Simulation, Beijing, China
[2]Earth and Environmental Sciences Division, Los Alamos National Laboratory, Los Alamos, New Mexico, United States
[3]College of Construction Engineering, Jilin University, Changchun, 130021, China
[4] Beijing Institute of Hydrogeology and Engineering Geology, Beijing, China
[5] Department of Civil, Environmental and Architectural Engineering, University of Padova, Italy

Correspondence to: Lin Zhu hi-zhulin@163.com; Huili Gong gonghl@263.com

Abstract. Alluvial fans are highly heterogeneous in hydraulic properties due to complex depositional processes, which make it difficult to characterize the spatial distribution of the hydraulic conductivity (K). An original methodology is developed to identify the spatial statistical parameters (mean, variance, correlation range) of the hydraulic conductivity in a three-dimensional setting by using geological and geophysical data. More specifically, a large number of inexpensive vertical electric soundings is integrated with a facies model developed from borehole lithologic data to simulate the $\log_{10}(K)$ continuous distributions in multiple-zone heterogeneous alluvial megafans. The Chaobai River alluvial fan in the Beijing Plain, China, is used as an example to test the proposed approach. Due to the non-stationary property of the K distribution in the alluvial fan, a multi-zone parameterization approach is applied to analyze the conductivity statistical properties of different hydrofacies in the various zones. The composite variance in each zone is computed to describe the evolution of the conductivity along the flow direction. Consistently with the scales of the sedimentary transport energy, the results show that conductivity variances of fine sand, medium-coarse sand, and gravel decrease from the upper (Zone 1) to the lower (Zone 3) portion along the flow direction. In Zone 1, sediments were moved by higher-energy flooding, which induces poor sorting and larger conductivity variances. The composite variance confirms this feature with statistically different facies from Zone 1 to Zone 3. The results of this study

provide insights to improve our understanding on conductivity heterogeneity and a method for characterizing the spatial distribution of *K* in alluvial fans.

1 Introduction

Alluvial fans usually house valuable groundwater resources because of significant water storage and favorable recharge conditions. Sedimentary processes forming alluvial fans are responsible for their complex long-term evolution. Usually, the coarsest material (gravel) is deposited in the upper fan, with the gravel passing into sand in the middle of the fan and then into silt and clay in the tail. A high heterogeneity characterizes the deposit distribution because of the shifting over time of the sediment-transporting streams (Zappa et al., 2006; Weissmann et al., 1999).

Hydraulic conductivity distributions in alluvial fans can be assigned according to the various hydrofacies simulated by conditional indicator geostatistical methods (Eggleston and Rojstaczer 1998; Fogg et al., 1998; Weissmann and Fogg, 1999; Weissmann et al., 2002a, 2002b; Ritzi et al., 2004, 2006; Proce et al., 2004; Dai et al., 2005; Harp et al., 2008; Hinnell et al., 2010; Maghrebi et al., 2015; Soltanian et al., 2015; Zhu et al., 2015a). However, the geostatistical methods require the stationary assumption, i.e. the distribution of the volumetric proportions and correlation lengths of hydrofacies converge to their mean values in the simulation domain. The hydrofacies and hydraulic conductivity (*K*) distributions in alluvial fans are generally non-stationary (Weissmann et al., 1999; Anderson, 2007; Weissmann et al., 2010, 2013; Zhu et al., 2016a). Hence, the use of these methods may cause large characterization errors and add significant uncertainty to the predictions achieved by groundwater flow and contaminant transport models (Eggleston and Rojstaczer 1998; Irving and Singha 2010; Dai et al., 2014a). Zhu et al., (2016a) adopted a local-stationary assumption by dividing the alluvial fan into three zones along the flow direction of the Chaobai River, China. The zones were properly detected based on the statistical facies distribution. Then, the indicator simulation method was applied to each zone and the simulated hydrofacies distribution in the three zones was used to guide modelling the *K* distribution. Hydraulic conductivity of granular deposits generally varies with grain size, porosity, and sorting. Traditional methods for *K* estimate, e.g. well test, permeability measurements, and grain-size analyses (Niwas et al., 2011), are very expensive, time-consuming, and make difficult to provide representative and sufficient field data for addressing spatial variations of conductivity. Recently, data fusion techniques have been developed for coupled inversion of multi-source data to estimate *K* distributions for groundwater numerical modeling. Geophysical data (such as surface electric resistivity and various logging data) are relatively inexpensive and can provide considerable information for characterizing subsurface heterogeneous properties (Hubbard et al., 2001; Yeh et al., 2002; Dai et al., 2004a; Morin 2006; Sikandar et al., 2010; Bevington et al., 2016). Electric resistivity data have been proven useful to derive sediment porosity distributions (Niwas and Singhal 1985; Niwas et al., 2011; Niwas and Celik 2012; Zhu et al., 2016b). Zhu et al. (2016b) simulated the spatial distributions of hydraulic conductivity by combing the interpolated resistivity on basis of VES and the stochastic simulated facies through empirical equation, in which the hydraulic conductivity was converted from the porosity data calculated from resistivity measurements and the grain size.

This study proposes a novel approach to reconstruct the three-dimensional configuration of conductivity in alluvial fans by combining the hydrofacies spatial heterogeneity provided by a multi-zone transition probability model with hydrogeological and hydrogeophysical measurements, in particular inexpensive vertical electrical soundings (VES) properly calibrated through resistivity logs acquired in a few wellbores. We assume the K distributions are local-stationary, i.e. the mean and variance of log conductivity are convergent in each hydrofacies and in each local zone. Therefore, we can compute the $\log_{10}(K)$ semivariogram in each hydrofacies and in each zone. The spatial structure features of hydraulic conductivity deduced from semivariograms are used during the geostatistical simulation processes of the hydraulic conductivity. The Chaobai alluvial fan (or called "megafan" as defined by Leier et al. (2005) and Hartley et al. (2010) for very large alluvial fans) in the northern Beijing Plain, China, was selected as study area to test the proposed integrated approach.

2 Material and Methods

2.1 Study area

The study area belongs to the Chaobai River alluvial fan (or megafan), in the northern Beijing Plain (northern latitude 40°-40°30′, eastern longitude 116°30′-117°), with an area of 1,150 km^2 (Fig. 1a). The Chaobai River is the second largest river flowing through the Beijing Plain from north to south. The ground elevation decreases southward with an average 2‰ slope. Quaternary sediments were mainly deposited by flooding events with turbulent flow and consist of porous strata containing groundwater. The aquifer system in the alluvial fan can be divided into three zones according to the lithological features (Fig. 1): an upper fan zone (or Zone 1) with coarse sediments (e.g., sandy-gravel aquifers), a middle upper fan zone (or Zone 2) where medium-coarse sediments (e.g., sandy-gravel to sandy-silt aquifers) were deposited , and a fine-sediment (e.g., sand and clay multiple aquifers) middle-lower fan zone (or Zone 3). Four hydrofacies, including sub-clay and clay (C), fine sand (FS), medium-coarse sand (MS), and gravel (G), were classified based on the interpretations of the cores and textural description of almost 700 boreholes (Zhu et al., 2015).

The study area is one of the most important regions for the supply of groundwater resource to Beijing. The Huairou emergency groundwater resource region (hereafter EGRR) with an area of 54 Km^2 is located in Zone 1. The total groundwater withdrawal amounted to 1.2×10^8 m^3 in 2003. Several well-fields belonging to the so-called "water supply factory" were drilled along the Chaobai River in Zone 1 and the upper Zone 2. Most of these well-fields were built in 1979 with a designed groundwater pumping volume of 1.6×10^8 m^3 per year. The average thickness of the exploited aquifer system is approximately 300 m. The long-term over-exploitation of the aquifer system has resulted in a serious drawdown of water levels, which has reduced the exploitable groundwater resources and induced geological disasters, mainly land subsidence, fault reactivation, and ground fissures (Cheng et al., 2015; Yang et al., 2015; Zhu et al., 2015). In 2010, the annual groundwater withdrawal at the EGRR and the water factory decreased to 0.86×10^8 m^3 and 0.65×10^8 m^3, respectively.

The largest cumulative land subsidence from June 2003 to January 2010 was quantified in approximately 340 mm by Zhu et al., (2013, 2015) in Tianzhu County to the south. The characterization of the distribution and spatial variability of the hydraulic conductivity is vital for an optimal use of the limited water resources in this area.

2.2 Methodological approach

Nowadays, a large set of hydraulic conductivity samples can be derived by integrating appropriate relations of various geological data, including hydrogeophysical measurements, borehole lithostratigraphies, and hydrogeological information (total dissolved solid TDS and groundwater level). These databases can be statistically processed to derive the spatial variation of $\log_{10}(K)$ for various facies, including clay, fine sand, medium-coarse sand, and gravel.

In this paper, the statistical assessment is separately carried out for separated zones, building-up experimental semivariograms that are fitted with exponential models. The optimal parameters of these latter are estimated through a generalized output least squares (OLS) criterion. Then, the composite semivariograms are computed using a hierarchical sedimentary architecture (Ritzi et al., 2004; Dai et al., 2005) to obtain the K variance in each zone. Finally, the configuration of $\log_{10}(K)$ is simulated through a multiple-zone sequential Gaussian algorithm with estimated statistic parameters reflecting the K spatial structures in the alluvial fan. Figure 2 shows the steps involved in the developed approach.

2.3 Data set

2.3.1 Geophysical data

Geophysical data include resistivity loggings and vertical electrical soundings. There are six well-electric logs continuously recording the formation resistivity versus depth. Five logs were collected in Zone 2 and one in Zone 3. Each well log has a lithological description, which helps to relate the resistivity values to the corresponding facies.

The average resistivity of G is the largest, with a value of 198 Ω m, and that of C is the smallest with a value of 24 Ω m. Figure 3 compares the outcome of logging data in term of resistivity versus depth and the corresponding stratigraphy, where the groundwater depth is 12 m. The log was acquired in the eastern part of Zone 2. The average resistivity from 32.4 m to 40.5 m depth, where the sediments are mainly G and MS, is 70.8 Ω m. The resistivity curve shows two evident peaks from 97 m to 102 m and between 81 m and 84.5 m depth, where the MS is located.

The C resistivity is relatively low due to the good intrinsic electrical conductivity of this facies. For example from 16.5 m to 23.5 m depth, where C is the prevalent facies, a low resistivity equal to 27.2 Ω m is recorded. Since a hydrofacies with a smaller grain size has a greater total surface area, the resistivity difference can partially reflect the distributions of particle sizes and the hydrofacies composition. Since the obtained resistivity is the apparent resistivity, we used the resistivity located in the middle of the facies block, where the resistivity is approximate to the real resistivity. Unfortunately, it is unknown to the authors if the logs were calibrated in the field and how the salinity of the formation water, although minimal and almost independent on the site and depth, has been accounted for. On the other hand, the resistivity distributions have good correlations with different hydrofacies along the vertical and horizontal directions. Therefore, in the mathematical framework that follows, we have assumed that the logs have been calibrated and are accurate enough for presenting our work as a proof of concept.

Vertical electrical soundings (VES) using the Schlumberger electrode configuration were carried out by the Beijing Institute of Hydrogeology and Engineering Geology (BIHEG). A number of 113 detecting positions were selected, with a maximum half current electrode space equal to 340 m and the potential electrode space ranging from 1 to 30 m. All the sounding data (1356 VES measurements) recorded the apparent resistivity of the porous medium. These data were inverted to real resistivity using the nonlinear Occam inversion method (Constable et al., 1987), with a low root mean square relative error of 2%. Figure 4 shows the layered structure fitting model of resistivity and the borehole lithologic observations. The inversed resistivity generally reflects the difference of facies: the thick gravel layer has larger resistivity while the fine sand and clay layers have relatively smaller resistivity.

2.3.2 Geological and hydrogeological data

Almost 700 borehole lithologic logs were collected in the study area. The sedimentary deposits show large heterogeneity from the upper to the lower fan zone. In Zone 1, the dominant facies is G with a volumetric proportion of 53%. The volumetric proportion of C is 16%. In Zone 2, the volumetric proportion of C increases to 40%, while that of G decreases sharply to 24%. In Zone 3, the proportion of G decreases further to 6% and that of C increases to 50% (Table 1). More detailed information is given in Zhu et al., (2016a). The lithological information in a buffer zone of 200 m around the VES locations has been used to represent the actual facies distribution in the area surrounding the sites of the geophysical acquisitions.

A number of 35 hydrochemistry measurements with a depth from 20 m to 270 m were obtained throughout the area. The minimum, maximum and average TDS values are 423 mg/l at the depth of 180 m, 943 mg/l at the depth of 50 m, and 692 mg/l, respectively. Generally, the TDS is very low with the higher values measured in the south-western part of the study area. Because of the relatively small dataset and the observed low variability, in this paper the TDS variation in the vertical direction has been neglected. A TDS map was obtained by interpolating the available records using an Ordinary Kriging method with a spherical semivariogram model.

A large number of depth of water level measurements were also collected to map the thickness of the unsaturated unit. The TDS and groundwater level at each VES and resistivity log location were derived from the interpolated surfaces.

2.3.3 Hydraulic conductivity estimates from geophysical acquisitions

The hydraulic conductivity *K* was estimated using the Kozeny-Carman equation:

$$K(x,y,z) = \frac{\delta g}{\mu} \times \frac{d^2_{(x,y,z)}}{180} \frac{\phi^3_{(x,y,z)}}{(1-\phi_{(x,y,z)})^2} \quad (1)$$

which is widely accepted to derive the hydraulic conductivity from grain size and porosity (Soupious et al., 2007; Utom et al., 2013; Khalil et al., 2013; Zhu et al., 2016). In Eq. (1), $d_{(x,y,z)}$ is the median grain diameter (D50, mm) at location (*x*,*y*,*z*), which was determined according to the lithology information (or lithological descriptions and grain size distributions), g is gravity, μ the kinematic viscosity (kg/(m·s)), δ the fluid density, and $\phi_{(x,y,z)}$ the porosity. ϕ was estimated using Archie's law (Eq. (2)), which relates the bulk resistivity of granular medium to porosity:

$$\rho = \alpha \rho_w \phi^{-m} s_w^{-n} \quad (2)$$

where ρ is the saturated formation resistivity (Ω m), α the pore-geometry coefficient associated with the medium ($0.5 \leq \alpha \leq 2.5$), m the cementation factor ($1.3 \leq m \leq 2.5$) (Massoud et al., 2010; Khalil and Santos 2013). α is set as 1. In the upper part of alluvial (Zone 1 and Zone 2) m is set as 1.3 due to the sand is unconsolidated. In Zone 3 m is set as 1.7 which reflects slightly cemented sandstones (Niwas et al. 2011). s_w the water saturation, and n the saturation index. The pore fluid resistivity (Ω m) ρ_w is calculated using the following experimental relation:

$$\rho_{\mathrm{w}} = \frac{5.6(\mathrm{TDS})^{b}}{1+\beta(\mathrm{t}-18)} \tag{3}$$

with TDS in (g/L), temperature t in (°C), b and β being constant parameters (Wu et al., 2003). For the most common electrolytes, b = -0.95 and β = 0.025. Note that the parameters associated with equations (2) and (3) are site specific and application these equations to other sites will need re-adjust the related parameters.

The logarithmically transformed values of the estimated hydraulic conductivity ($\log_{10}(K)$) were used for the geostatistical analysis because of its normal distribution (Neuman, 1990). The histograms of $\log_{10}(K)$ values within each facies are in Fig. 5. There are 102, 2077, and 1716 conductivity samples in Zone 1, Zone 2, and Zone 3, respectively. Considering that Archie's law can only be used for clay-free granular sediments, the K values of C were not estimated in this study. Based on the lithological description information of borehole data, it has been reasonably assumed that clay fraction is negligible in G, MS, and FS facies. The statistics of $\log_{10}(K)$ for the three facies in three zones are listed in Table 2. The mean $\log_{10}(K)$ values decrease from Zone 1 to Zone 3, consistently with the sedimentary transport processes in the alluvial fan. In the upper region (Zone 1), high water flowing energy made the deposits consisted mainly of larger-grained particles and the coarse-grained sediments are dominant. In the southern part (Zone 3), the deposits change to relatively fine-grained particles. The mean $\log_{10}(K)$ of gravel is greater than 2.4 (log(m/d)) and that of fine sand is less than 0.2 (log(m/d)). The lithological information at the depth of the conductivity samples shows that volumetric proportions of FS and MS increase and that of G decreases from Zone 1 to Zone 3. The results are consistent with the statistic outputs deduced from 694 borehole data by Zhu et al., (2016a).

2.4 Statistical Methods

2.4.1 Semivariogram of hydraulic conductivity

Semivariogram describes the degree of spatial dependence of a spatial random field or stochastic process. It is a concise and unbiased characterization of the spatial structure of regionalized variables, which is important in Kriging interpolations and conditional simulations. The experimental semivariogram:

$$\hat{r}_k(h_\varphi) = \frac{1}{2N(h)} \sum_{(o,p)\in N(h)} (Y(z_o) - Y(z_p))^2 \quad (4)$$

can be fitted by an exponential model (e.g., Dai et al., 2014b):

$$r_k(h_\varphi) = \sigma^2 (1 - e^{\frac{-3h}{\lambda}}) \quad (5)$$

where $\hat{r}_k(h_\varphi)$ and $r_k(h_\varphi)$ are the experimental and model semivarograms of log conductivity Y for the k^{th} facies at a lag distance h along the φ direction. In this paper we calculate the semivarograms in the vertical and dip directions. $N(h)$ is the number of pair measuring points z_o and z_p separated by a h lag distance, σ^2 is the variance, and λ the correlation range.

The variance and range were optimized using the least-squares criterion, which was solved by the modified Gauss-Newton-Levenberg-Marquardt method (Clifton and Neuman, 1982; Dai et al., 2012). The sensitivity equation method was derived to compute the Jacobian matrix for iteratively solving the gradient-based optimization problem (Samper and Neuman 1986; Carrera and Neuman 1986; Dai and

Samper, 2004; Samper et al., 2006; Yang et al., 2014; Zhu et al., 2016a). The two sensitivity coefficients $\frac{\partial r_k}{\partial \sigma^2}$ and $\frac{\partial r_k}{\partial \lambda}$ are the partial derivatives of the semivariogram with respect to variance and range:

$$\frac{\partial r_k}{\partial \sigma^2} = 1 - e^{\frac{-3h}{\lambda}} \quad (6)$$

$$\frac{\partial r_k}{\partial \lambda} = -\sigma^2 \cdot 3h \cdot e^{\frac{-3h}{\lambda}} \cdot \lambda^{-2} \quad (7)$$

2.4.2 Composite semivariogram of log conductivity

Once the facies semivariograms were obtained in each zone, the composite semivariogram $\gamma(h)$ could be calculated through the following equation (e.g., Ritzi et al., 2004):

$$\gamma\left(h_\varphi\right) = \sum_{k=1}^{M} \sum_{i=1}^{M} r_{ki}(h_\varphi) p_k t_{ki}(h_\varphi) \quad (8)$$

where p_k and $t_{ki}(h_\varphi)$ are the volumetric proportion of facies k and the transition probability from facies k to facies i in the φ direction with a h lag distance, respectively. Equation 8 delineates the composite semivarigoram with respect to the individual facies semivariogram and transition probability. The general shape function and range of the composite semivarigoram can be obtained from individual facies mean length and volumetric proportion with the methods described in Dai et al., (2005).

The transition probability $t_{ki}(h_\varphi)$ has an analytical solution as derived by Dai et al., (2007):

$$t_{ki}\left(h_\varphi\right) = p_k + (\delta_{ki} - p_k) \cdot \exp\left(\frac{h_\varphi}{\lambda_\varphi}\right) \quad (9)$$

where δ_{ki} is the Kronecker delta and λ_φ is the integral scale in the direction of φ. A geostatistical modeling tool GEOST (Dai et al., 2014b) modified from the Geostatistical Software Library (Deutsch and Journel, 1992) and TPROGS (Carle and Fogg, 1997) was employed to compute the sample transition probabilities in each zone. The parameters p_k and λ_φ were optimally estimated through a modified Gauss-Newton-Levenberg-Marquardt method. More details are provided by Zhu et al., (2016a). The composite semivariograms for different zones can help us to understand the heterogeneity variations from the upper to lower part of the alluvial fan, as well as the stationary property (local versus regional) of the facies and hydraulic conductivity distributions.

2.4.3 Sequential Gaussian simulation

The Sequential Gaussian simulation (SGSIM) is a widely used stochastic simulation method to create numerical model of continuous variables based on the Gaussian probability density function. The process is assumed to be a stationary and ergodic random process (Deutsch and Journel, 1992; Dimitrakopoulos and Luo, 2004). This method can preserve the variance and correlation range observed in spatial samples. SGSIM provides a standardized normal continuous distribution of the simulated variable.

With the assumption that the log conductivity distributions are stationary within each zone, we used SGSIM simulator implemented into GEOST to model the $\log_{10}(K)$ continuous configuration under a multiple-zone framework. The conductivity of the FS, MS, and G facies in each zone was simulated sequentially using the structure characteristics of the semivariograms.

Finally, the three-dimensional conductivity configuration was derived by combining the stochastic simulated facies (Zhu et al., 2016a) with the SGSIM conductivity distribution and the mean $\log_{10}(K)$ of the various facies in each zone (Table 2). The stochastic simulated facies was constructed through the optimized volumetric proportion and mean length of facies in three directions. The mean length in vertical and dip directions were calculated through 694 borehole. The mean length in strike direction was assumed as half as that in dip direction. During the facies simulation process, borehole data were used as conditional data (Zhu et al., 2016a). In detail, since each cell is characterized by specific facies and zone indices, its conductivity was assigned using the corresponding (in relation to the facies and the zone) 3D SGSIM outcome in that position. Note that The hydrofacies (e.g., C, FS, MS and G) are defined qualitatively based on the sedimentary structures, borehole lithological descriptions, and grain sizes, while the conductivity samples are then deduced from geophysical measurements for each facies at each zone. Since the clay contents from zone 1 to zone 3 are increased due to the changes in the sediment transport conditions, for the same facies we also found this trend and the overall hydraulic conductivities are decreased from zone 1 to zone 3. Since sub-clay and clay are generally characterized by a low hydraulic conductivity value, a uniform K value equal to 0.0001 m/d was set to all the C cells.

3 Results and Discussion

3.1 Variation of $\log_{10}(K)$ for the various facies

The optimized vertical correlation range and variance of the log conductivity semivariogram (Eq. 5) are listed in Table 3, along with their 95% confidence intervals. The fitting between the experimental and the model semivariograms is the best in Zone 2 because of the abundant samples, while the fitting in

Zone 1 is the worst (Fig. 6). The fitting result of the semivariogram for the G facies is the worst in Zone 1. Two are the reasons: the first is the high variance of the log conductivity of gravel in this zone; the other is the limited number of samples (102 samples), which makes quite small the pair numbers within each lag spacing. Hence, the computed semivariogram is highly uncertain.

The variance of FS, MS, and G in the vertical direction decreases from Zone 1 to Zone 3. In the upper alluvial fan, sediments were deposited under multiple water flowing events and with poor sorting. The deposits consist of wide ranges of sediment categories and grain sizes. The variance of G is larger than 1.5, which reflects the high heterogeneity of hydraulic conductivity in coarse deposits. The variances of FS and MS are smaller with values equal to 0.23 and 0.32, respectively. In Zone 3, these values decrease to 0.05 and 0.13, respectively, with that of G sharply decreasing to 0.62. In the middle-lower fan zone, the conductivity variation within each facies reduces gradually because the ground surface slope becomes smaller or flat, the sediment transport energy decreases, and the deposits within the three facies are well sorted.

Note that the ranges are correlated with the facies structure parameters such as the indicator correlation scale, mean thickness (or length), and volumetric proportion (Dai et al., 2004b; 2007). The estimated correlation ranges of FS, MS and G along the vertical direction in Zone 1 do not show big difference with values equal to 6.0 m, 8.0 m and 6.5 m, respectively. Zone 2 was extended from the fan apex zone (Zone 1) with much larger area, which allows for greater preservation potential of finer sediments (such as medium-coarse sand (MS), fine sand (FS), and clay or sub clay (C)) than the more proximal Zone 1. Therefore, in Zone 2 the volumetric proportions for these three facies increase while that of gravel decreases. The estimated ranges of G and MS are increased, respectively. In Zone 3, the range difference among the three facies decreases gradually. The range of FS is about 6.0 m, which is twice as much as that of MS. The spatial variation of the structure parameters of three facies causes the large changes of the correlation ranges from Zone 1 to Zone 3.

Due to the small number of conductivity samples in Zone 1, the variance of $\log_{10}(K)$ along the dip direction is calculated only in Zone 2 and Zone 3 (Table 4, Fig. 7), as observed along the vertical direction. This phenomenon possibly reflects that sediment transport energy decrease along the flow direction. Lower energy flow in Zone 3 cause better sediment sorting and weak heterogeneity (or lower variance) in hydraulic conductivity.

3.2 Composited semivariogram of $\log_{10}(K)$

The composite semivariogram in the vertical direction at each zone is calculated by Eq. (8), using the volume proportions (Table 1) and transition probability (Eq. (9)) with the same values of the lag distance used to compute the facies semivariograms (Fig. 8). The values of the optimized variance are 0.68, 0.11, and 0.03 in Zone 1, Zone 2, and Zone 3, respectively. The high flow energy and the large number of flooding events contributing to sediment deposition are the main causes of the high heterogeneity (largest variance) of the deposits in the upper part of the alluvial fan. The changes of variance between the three zones support the utilization of the local-stationary assumption and simulation of multiple-zone based conductivity distributions for the Chaobai alluvial fan.

3.3 Configuration of $\log_{10}(K)$

The configuration of $\log_{10}(K)$ in three dimensions is showed in Fig.9. The distribution of conductivity is generally consistent with that of the facies. Coarse units are more frequently distributed in the upper zone, which makes the average K is much larger in this zone than that in the lower part of the alluvial fan. The regions with high conductivity (red color in Fig. 8) in Zone 1 are more continuous than that in other parts. The adjacent cells with the smallest conductivity (blue color in Fig. 8) are obviously located mainly in Zone 3. The mean conductivity is smaller in the southern part of the study area, where the piezometric drawdowns in the multi-layer aquifer system were larger and the surface subsidence more serious (Zhu et al., 2013, 2015). Note that since we simulated the dip direction along the main water flow direction and, due to the lack of enough data, the strike-directional semivariogram is assumed to be similar as that in dip direction, the simulated facies in the fan apex did not show a radiating pattern. More information about simulating the radiating pattern can be found from Carle et al. (1997) and Fogg et al. (1998).

Based on the three dimensional K configuration, the average value of K in the depth range from 0 m to 300 m amounts to 194 m/d, 25 m/d and 4 m/d in Zone 1, Zone 2, and Zone 3, respectively. These values are comparable with those provided by the Beijing Institute of Hydrogeology and Engineering Geology (2007) based on a number of pumping tests carried out over several years in the study area. In this BIHEG report the average value of K is $>$300 m/d in Zone 1, between 30 and 100 m/d in Zone 2, and $<$30 m/d in Zone 3 (Fig. 1b). The fact that the arithmetic average K values are gently smaller than these latter are likely due to the fact that the outcome of pumping tests are generally more representative of coarser sediments.

Investigating the stochastic results along the vertical direction, it is interesting to notice that the average K in deep units of Zone 1 and Zone 2 is smaller than that in the shallow strata. For example, in Zone 1 the average K for the cells from 0 m to 100 m deep is 295 m/d, which is three times as much the value for the depth range between 200 m and 300 m. Conversely, no significant variation of K versus depth is observed in Zone 3, with only a small decrease of the average K from the deeper to the shallower units.

4 Conclusions

This paper proposes a geostatistical method under a multiple zone framework, properly supported by a large number of geophysical investigations, to detect the distribution and the related variance of the hydraulic conductivity in three-dimensional domains. In particular, the optimized statistical parameters (e.g., log conductivity variance and correlation range) of semivariograms are estimated using the modified Gauss-Newton-Levenberg-Marquardt method. The Chaobai alluvial fan is used as a case study area. Multiple data including downhole resistivity logging data, vertical electric soundings, well-bore lithologic logs, TDS measurements, and depths to the water table are integrated to derive a dataset of conductivity values in a three-dimensional setting. Log conductivity semivariograms fitted with exponential functions were constructed for three facies, including fine sand, medium-coarse sand and gravel, in each of the three zones into which the Chaobai fan is divided to guarantee local stationarity of the statistical process. The composite semivariogram of the three facies has been derived for the two zones where a sufficiently large number of samples are available. The $\log_{10}(K)$ configuration is simulated using the sequential Gaussian simulation model based on statistic parameters of $\log_{10}(K)$ and the structure suggested by a 3D hydrofacies simulation.

For the specific test case, the variance along the vertical direction of fine sand, medium-coarse sand, and gravel decreases from the upper part of the alluvial fan, where the values amount to 0.23, 0.32, and 1.60, to the lower portion of the Chaobai plan with values of 0.05, 0.126, and 0.62, respectively. This behavior reflects the higher transport energy in the upper alluvial fan that causes a poor sediment sorting. In the middle alluvial fan, the transport energy decreases and the sediments tend to be relatively well-sorted. The variance of the gravel is larger than that of other lithologies. The different flow energy significantly affected the coarse sediments in the vertical direction. Along the dip direction, the variance of three facies (gravel, medium-coarse sand and fine sand) in the middle fan is larger than that in the lower fan. The composite variance of $\log_{10}(K)$ in the vertical direction shows that the large heterogeneity in the upper fan (with a value of 0.68) decreases in the lower zone.

The distribution of hydraulic conductivity is consistent with that of the facies. Hydraulic conductivity is much larger in the upper zone than that in the lower part of the alluvial fan. This result provides valuable insights for understanding the spatial variations of hydraulic conductivity and setting-up groundwater flow, transport, and land subsidence models in alluvial fans.

Concluding, it is worth highlighting that we depicted an original method to detect the variance and configuration of conductivity by fusing multiple-source data in three-dimensional domains. The proposed approach can be easily used to statistically characterize the hydraulic conductivity of the various alluvial fans that worldwide are strongly developed to provide high-quality water resources. We are aware of some restrictions in the dataset available at the date for the Chaobai alluvial fan, for example the assumed uniform distribution of TDS versus depth and the relatively small number of the conductivity samples in the upper fan zone. A more accurate description of the semivarigrams in the dip and lateral directions will be included in our future study to improve the developed three-dimensional permeability field. Moreover, our assumption that the logs are well-calibrated might be another source of uncertainty that can be reduced in our next-step work. Nonetheless, the proposed methodology will be re-applied in the near feature as soon as new information will become available, thus allowing to improve the estimation accuracy of spatial statistics parameters and the configuration of hydraulic conductivity in this Quaternary system so important for the Beijing water supply.

Data availability

The geophysical measurements, borehole lithostratigraphies, and hydrogeological information in the north part of Beijing Plain can be partly accessible by contacting Beijing Institute of Hydrogeology and Engineering Geology.

Author contribution

Lin Zhu, Huili Gong and Zhenxue Dai derived the method of spatial variance and 3D configuration of conductivity, performed data analysis and wrote the draft manuscript. Gaoxuan Guo collected the geological and geophysical data, discussed the results. Pietro Teatini discussed the results, reviewed and revised the manuscript.

Competing interests

The authors declare that they have no conflict of interest.

Acknowledgements

This work was supported by the National Natural Science Foundation (No.41201420, 41130744) and Beijing Nova Program (No.Z111106054511097). Pietro Teatini was partially supported by the University of Padova, Italy, within the 2016 International Cooperation Program.

References

Anderson, M.P.: Introducing groundwater physics, *Phys. Today*, 42–47, 2007

Beijing Institute of Hydrogeology and Engineering Geology: Groundwater flow model and the potential groundwater resources in Beijing Plain, Internal Report, 60-64., 2007 (In Chinese)

Bevington, J., Piragnolo, D., Teatini, P., Vellidis, G., and Morari, F.: On the spatial variability of soil hydraulic properties in a Holocene coastal farmland, *Geoderma*, 262: 294-305, doi:10.1016/j.geoderma.2015.08.025, 2016.

Carle, S.F., and Fogg, G.E.: Modeling spatial variability with one and multimensional continuous-lag Markov chain, *Math. Geol*., 29(7): 891-918, doi: 10.1023/a:1022303706942, 1997.

Carrera, J., and Neuman, S.P.: Estimation of aquifer parameters under steady state and transient condition: 2. Uniqueness, stability, and solution algorithms, *Water Resour. Res*., 22, 211 – 227, doi: 10.1029/wr022i002p00211, 1986.

Cheng, G., Wang, H., Luo, Y., and Guo, H.: Study of the deformation mechanism of the Gaoliying ground fissure: Prevention and Mitigation of Natural and Anthropogenic Hazards due to Land Subsidence - Proc. IX Int. Symp. on Land Subsidence, K. Daito et al. eds., Proc. IAHS, UK, 231-234, 2015.

Clifton, P.M., and Neuman, S.P.: Effects of kriging and inverse modeling on conditional simulation of the Avra Valley aquifer in southern Arizona, *Water Resour. Res*., 18, 1215-1234, doi: 10.1029/wr018i004p01215, 1982.

Constable, S.C., Parker, R.L., and Constable, C.G.: Occam’s inversion: A practical algorithm for generating smooth models from electromagnetic sounding data, *Geophysics*, 52, 289-300, 1987.

Dai, Z., and Samper, J.: Inverse problem of multicomponent reactive chemical transport in porous media: Formulation and applications, *Water Resour. Res*., 40, W07407, doi: 10.1029/2004wr003248, 2004.

Dai, Z., Ritzi, R., and Dominic, D.: Estimating parameters for hierarchical permeability correlation models. Aquifer Characterization, Bridge, J.S. and Hyndman, D.W. *SEPM Society for Sedimentary Geology*, USA, 41-54, doi: 10.2110/pec.04.80.0041, 2004a.

Dai, Z., Ritzi, R., Huang, C., Dominic, D., and Rubin, Y.: Transport in heterogeneous sediments with multimodal conductivity and hierarchical organization across scales, *J. of Hydrol.*, 294, 68-86, doi: 10.1007/s00477-014-0922-3, 2004b.

Dai Z., Ritzi, R., and Dominic, D.: Improving permeability semivariograms with transition probability models of hierarchical sedimentary architecture derived from outcrop analog studies. *Water Resour. Res.*, 14 W07032, doi: 10.1029/2004wr003515, 2005.

Dai, Z., Wolfsberg, A., Lu, Z., and Ritzi, R.: Representing aquifer architecture in macrodispersivity models with an analytical solution of the transition probability matrix. *Geophys. Res. Lett*., 34, L20406, doi: 10.1029/2007GL031608, 2007.

Dai, Z., Wolfsberg, A., Reimus, P., Deng, H., Kwicklis, E., Ding, M., Ware, D., and Ye, M.: Identification of sorption processes and parameters for radionuclide transport in fractured rock, *J. Hydrol.*, 414-415, 220-230, doi: 10.1016/j.jhydrol.2011.10.035, 2012.

Dai, Z., Stauffer, P. H., Carey, J. W., Middleton, R. S., Lu, Z., Jacobs, J. F., Hnottavange-Telleen, K. & Spangle, L. Pre-site characterization risk analysis for commercial-scale carbon sequestration. *Environ. Sci. Technol*. 48, 3908−3915, 2014a.

Dai, Z., Middleton, R., Viswanathan, H., Fessenden-Rahn, J., Bauman, J., Pawar, R., Lee, S., and McPherson, B.: An integrated framework for optimizing CO_2 sequestration and enhanced oil recovery. *Environ. Sci. Technol. Lett*., 1, 49-54, doi: 10.1021/ez4001033, 2014b.

Deutsch, C.V., and Journel, A.G. GSLIB: Geostatistical software library, Oxford Univ. Press. New York, 340, 1992.

Dimitrakopoulos, R., and Luo, X.: Generalized sequential Gaussian simulation on group size v and screen-effect approximations of large field simulations. *Math. Geol.*, 36, 567-590, doi: 10.1023/b:matg.0000037737.11615.df, 2004.

Eggleston, J., and Rojstaczer, S.: Identification of large-scale hydraulic conductivity trends and the influence of trends on contaminant transport. *Water Resour. Res.*, 34, 2155-2186, doi: 10.1029/98wr01475, 1998.

Fogg, G.E., Noyes, C.D., and Carle, S.F.: Geologically based model of heterogeneous hydraulic conductivity in an alluvial setting, *Hydrogeol. J.*, 6(1), 131-143, doi: 10.1007/s100400050139, 1998.

Harp, D., Dai, Z., Wolfsberg, A., and Vrugt, J.: Aquifer structure identification using stochastic inversion, *Geophys. Res. Lett.*, 35, L08404, doi: 10.1029/2008gl033585, 2008.

Hartley, A.J., Weissmann, G.S., Nichols, G.J., and Warwick, G.L., Distributive fluvial systems: characteristics, distribution, and controls on development, *J. of Sediment. Res.*, 79, 167-183, doi: 10.2110/jsr.2010.016, 2010.

Hinnell, A.C., Ferre, T.P.A., Vrugt, J., Huisman, J.A., Moysey, S., Rings, J., and Kowalsky, M.B.: Improved extraction of hydrologic information from geophysical data through coupled hydrogeophysical inversion. *Water Resour. Res.*, 46, doi: 10.1029/2008wr007060, 2010.

Hubbard, S.S., Chen, J.S., Peterson, J., Majer, E.L., Williams, K.H., Swift, D.J., Mailloux, B., and Rubin, Y.: Hydrogeological characterization of the South Oyster Bacterial Transport site using geophysical data, *Water Resour. Res.*, 37, 2431-2456, doi: 10.1029/2001wr000279, 2001.

Irving, J., and Singha, K.: Stochastic inversion of tracer test and electrical geophysical data to estimatehydraulic conductivities, *Water Resour. Res.*, 46, W11514, doi: 10.1029/2009WR008340, 2010.

Khalil, M.A., and Santos, F.A.M.: Hydraulic conductivity estimation from resistivity logs: a case study in Nubian sandstone aquifer. *Arab. J. Geosci.*, 6, 205-212. doi: 10.1007/s12517-011-0343-2, 2013.

Leier, A.L., P. G. DeCelles, J. D. Pelletier, Mountains, monsoons, and megafans, *Geology,* 33, 289-292. doi: 10.1130/G21228.1, 2005.

Maghrebi, M., Jankovic, I., Weissmann, G.S., Matott, L.S., Allen-King, R.M., and Rabideau, A.J., Contaminant tailing in highly heterogeneous porous formations: Sensitivity on model selection and material properties. *J. of Hydrol.*, 531, 149-160. doi: 10.1016/j.jhydrol.2015.07.015, 2015.

Massoud, U., Santos, F.A.M., Khalil, M. A., Taha, A., and Abbas, A. M.: Estimation of aquifer hydraulic parameters from surface geophysical measurements: a case study of the Upper Cretaceous aquifer, central Sinai, Egypt, *Hydrogeol. J*., 18, 699-710, doi: 10.1007/s10040-009-0551-y, 2010.

Morin, R.H.: Negative correlation between porosity and hydraulic conductivity in sand-and-gravel aquifers at Cape Cod, Massachusetts, USA, *J. Hydrol*., 316, 43-52, doi:10.1016/j.jhydrol.2005.04.013, 2006.

Neuman, S.P.: Universal scaling of hydraulic conductivities and dispersivities in geologic media, *Water Resour. Res*., 26, 1749-1758, 1990.

Niwas, S., and Singhal, D.C.: Aquifer transmissivity of porous media from resistivity data, *J. Hydrol*., 82, 143-153, doi: 10.1016/0022-1694(85)90050-2, 1985.

Niwas, S., Tezkan, B., and Israil, M.: Aquifer hydraulic conductivity estimation from surface geoelectrical measurements for Krauthausen test site, Germany, *Hydrogeol. J*., 19, 307-315, doi: 10.1007/s10040-010-0689-7, 2011.

Niwas, S., and Celik, M.: Equation estimation of porosity and hydraulic conductivity of Ruhrtal aquifer in Germany using near surface geophysics. *J. Appl. Geophys*., 84, 77-85, doi: 10.1016/j.jappgeo.2012.06.001, 2012.

Proce, C., Ritzi, R. W., Dominic, D., and Dai, Z.: Modeling multiscale heterogeneity and aquifer interconnectivity, *Ground Water*, 42, 658-670, 2004.

Ritzi R., Dai, Z., Dominic, D., Rubin Y.: Reply to comment by Shlomo P. Neuman on “Spatial correlation of permeability in cross-stratified sediment with hierarchical architecture”. *Water Resour. Res.*, 42, W05602, doi:10.1029/2005WR004402, 2006.

Ritzi R., Dai, Z., and Dominic, D.: Spatial correlation of permeability in cross-stratified sediment with hierarchical architecture. *Water Resour. Res*., 40, W03513, doi: 10.1029/2003wr002420, 2004.

Samper, F.J., and Neuman, S.P.: Adjoint state equations for advective-dispersive transport: Proceeding of the 6th International Conference in Finite Elements in Water Resource, 423-437, New York, doi: 10.1007/978-3-662-11744-6_31, 1986.

Samper, J., Dai, Z., Molinero, J., García-Gutiérrez, M., Missana, T., and Mingarro, M.: Inverse modeling of tracer experiments in FEBEX compacted Ca-bentonite. *Physics and Chemistry of the Earth*, 31, 640-648, 2006.

Sikandar, P., Bakhsh, A., Arshad, M., and Rana, T.: The use of vertical electrical sounding resistivity method for the location of low salinity groundwater for irrigation in Chaj and Rachna Doabs, *Environ. Earth Sci.*, 60, 1113-1129, doi: 10.1007/s12665-009-0255-6, 2010.

Soltanian, M.R., Ritzi, R.W., Huang, C.C., and Dai, Z.: Relating reactive solute transport to hierarchical and multiscale sedimentary architecture in a Lagrangian-based transport model: 2: Particle displacement variance. *Water Resour. Res.*, 51, 1601-1618, doi: 10.1002/2014wr016354, 2015.

Soupios, P.M., Kouli, M., Vallianatos, F., Vafidis, A., and Stavroulakis, G.: Estimation of aquifer hydraulic parameters from surficial geophysical methods: A case study of Keritis Basin in Chania (Crete-Greece), *J. Hydrol*., 338, 122-131, doi: 10.1016/j.jhydrol.2007.02.028, 2007.

Utom, A.U., Odoh, B.I., Egboka, B.C.E., Egboka, N.E., and Okeke, H.C.: Estimation of subsurface hydrological parameters around Akwuke, Enugu, Nigeria using surface resistivity measurements. *J. Geophys. Eng*., 10, 025016, doi: 10.1088/1742-2132/10/2/025016, 2013.

Weissmann, G.S., and Fogg, G.E.: Multi-scale alluvial fan heterogeneity modeled with transition probability geostatistics in asequence stratigraphic framework. *J. Hydrol*., 226, 48–65, doi: 10.1016/S0022-1694(99)00160-2, 1999.

Weissmann, G.S., S.F. Carle, G.E. Fogg, Three-dimensional hydrofacies modeling based on soil surveys and transition probability geostatistics, *Water Resour. Res.*,35(6), 1761–1770, 1999.

Weissmann, G.S., Yong, Z., Fogg, G.E., Blake, R.G., Noyes, C.D., and Maley, M.: Modeling alluvial fan aquifer heterogeneity at multiple scales through stratigraphic assessment. Proceedings of the International Groundwater Symposium: Bridging the gap between measurement and modeling in heterogeneous media, Lawrence Berkeley National Laboratory, Berkeley, California, p25-28, 2002a.

Weissmann, G.S., Mount, J.F., and Fogg, G.E.: Glacially driven cycles in accumulation space and sequence stratigraphy of a stream-dominated alluvial fan, San Joaquin Valley, California, USA, *J. of Sediment. Res.* 72 (2), 240-251, 2002b.

Weissmann, G.S., Hartley, A.J., Nichols, G.J., Scuderi, L.A., Olson, M., Buehler, H., and Banteah, R., Fluvial form in modern continental sedimentary basins: the distributive fluvial system (DFS) paradigm: *Geology*, 38, 39-42, doi: 10.1130/G30242.1, 2010.

Weissmann, G.S., Hartley, A.J., Scuderi, L.A., Nichols, G.J., Davidson, S.K., Owen, A., Atchley, S.C., Bhattacharyya, P., Chakraborty, T., Ghosh, P., Nordt, L.C., Michel, L., and Tabor, N.J., Prograding distributive fluvial systems – geomorphic models and ancient examples, in Driese, S.G., and Nordt, L.C. (eds), *New Frontiers in Paleopedology and Terrestrial Paleoclimatology*, SEPM Special Publication No. 104, p. 131-147, 2013.

Wu, Y., Guo, J., and Qiang, J.: Assessing the total dissolved solid in groundwater on basis of resistivity. Conference on Groundwater Survey and Monitoring Technology, Baoding Hebei, China, 2003. (In Chinese)

Yang, C., Dai, Z., Romanak, K., Hovorka, S., and Trevino, R.: Inverse Modeling of Water-Rock-CO_2 Batch Experiments: Implications for Potential Impacts on Groundwater Resources at Carbon Sequestration Sites, *Environ. Sci. Technol*., 48, 2798–2806, doi: 10.1021/es4041368, 2014.

Yang, Y., Luo, Y., Liu, M., Wang, R., and Wang, H.: Research of features related to land subsidence and ground fissure disasters in the Beijing Plain: Prevention and Mitigation of Natural and Anthropogenic Hazards due to Land Subsidence - Proc. IX Int. Symp. on Land Subsidence, K. Daito et al. eds., Proc. IAHS,UK, 372, 239-242, 2015.

Yeh, T.C., Liu, S., Glass, R.J., Baker, K., Brainard, J.R., Alumbaugh, D., and LaBrecque, D.: A geostatistically based inverse model for electrical resistivity surveys and its applications to vadose zone hydrology. *Water Resour. Res.*, 38, 1278, doi: 10.1029/2001wr001204, 2002.

Zappa, G., Bersezio, R., Felletti, F., and Giudici, M.: Modeling heterogeneity of gravel-sand, braided stream, alluvial aquifers at the facies scale. *J. Hydrol.*, 325,134-153, doi :10.1016/j.jhydrol.2005.10.016, 2006.

Zhu, L., Gong, H., Li, X., Li, Y., Su, X., and Guo, G.: Comprehensive analysis and artificial intelligent simulation of land subsidence of Beijing, China. *Chin. Geogra. Sci.*, 23, 237–248, doi: 10.1007/s11769-013-0589-6, 2013.

Zhu, L., Gong, H., Li, X., Wang, R., Chen, B., Dai, Z., and Teatini, P.: Land subsidence due to groundwater withdrawal in the northern Beijing plain, China, *Eng. Geol.*, 193, 243-255, doi: 10.1016/j.enggeo.2015.04.020, 2015.

Zhu, L., Dai, Z., Gong, H., Gable, C., and Teatini, P.: Statistic inversion of multi-zone transition probability models for aquifer characterization in alluvial fans. *Stoch. Environ. Res. Risk Assess.*, 30, 1005-1016, doi: 10.1007/s00477-015-1089-2, 2016a.

Zhu, L., Gong, H., Chen, Y., Li, X., Chang, X., and Cui, Y.: Improved estimation of hydraulic conductivity by combining stochastically simulated hydrofacies with geophysical data. *Sci. Rep.*, 6, 22224, doi: 10.1038/srep22224, 2016b.

Table 1 Values of the volumetric proportion for the various facies in three zones

Zone	Sub-clay and clay	Fine sand	Medium-coarse sand	Gravel
Zone 1	0.166	0.234	0.067	0.533
Zone 2	0.409	0.286	0.065	0.240
Zone3	0.503	0.328	0.106	0.063

Table 2 Statistical data of logarithm hydraulic conductivity ($\log_{10}$(m/d)) in the three zones of the Chaobai alluvial fan

Zone	Parameter	Fine sand	Medium-coarse sand	Gravel
	Mean	**1.07**	**1.82**	**2.92**
Zone 1	Minimum	-0.94	1.22	2.26
	Maximum	1.65	2.45	3.66
	Proportion	0.36	0.12	0.32
	Mean	**0.42**	**1.17**	**2.65**
Zone 2	Minimum	-2.22	-0.23	0.95
	Maximum	1.22	2.07	3.38
	Proportion	0.23	0.14	0.31
	Mean	**0.17**	**0.81**	**2.48**
Zone 3	Minimum	-2.64	-0.78	0.34
	Maximum	0.72	1.43	3.21
	Proportion	0.35	0.17	0.12

Table 3 Optimized parameters in the fitting exponential function of $\log_{10}(K)$ semivariogram in vertical direction for the various facies and zones

Zone	Parameter	Fine sand		Medium-coarse sand		Gravel	
		Estimated value	Confidence Interval (95%)	Estimated value	Confidence Interval (95%)	Estimated value	Confidence Interval (95%)
Zone 1	Variance	0.23	(0.19, 0.28)	0.32	(0.29, 0.34)	**1.60**	(1.41, 1. 81)
	Range (m)	6.01	(2.01, 20.52)	8.01	(1.53, 14.67)	6.50	(6.50, 12.84)
Zone 2	Variance	0.069	(0.067, 0.070)	**0.14**	(0.13, 0.15)	**1.22**	(1.19, 1.24)
	Range (m)	3.13	(1.83, 4.42)	8.27	(3.61, 12.93)	15.0	(12.33, 17.67)
Zone3	Variance	0.05	(0.047, 0.053)	**0.126**	(0.118, 0.135)	**0.62**	(0.54, 0.7)
	Range (m)	6.52	(2.19, 10.85)	2.72	(0.20, 6.55)	5.98	(0.20, 15.63)

Table 4 Variances of $\log_{10}(K)$ of different facies along the dip direction in Zone 2 and Zone 3

Zone		Fine sand	Medium-coarse sand	Gravel
Zone 2	Estimated value	**0.10**	**0.15**	**1.38**
	Confidence Interval (95%)	(0.059, 0.141)	(0.071, 0.228)	(1.14, 1.62)
Zone 3	Estimated value	**0.045**	**0.068**	**0.48**
	Confidence Interval (95%)	(0.030, 0.0607)	(0.043, 0.093)	(0.22, 0.73)

Figure captions

Figure 1 Chaobai alluvial fan in the north of Beijing Plain. (a) Location of the study area and distribution of the field data. (b) Map of the hydraulic conductivity issued by Beijing Institute of Hydrogeology and Engineering Geology (2007). The location of the study area is shown in the inset.

Figure 2 Flowchart of the geostatistical methodology

Figure 3 Typical depth behaviors of resistivity and corresponding stratigraphy in the eastern part of Zone 2

Figure 4 Inversed resistivity and corresponding stratigraphy in Zone 1

Figure 5 Histograms of $\log_{10}K$ for fine sand, medium-coarse sand and gravel

Figure 6 Experimental (circle symbol) and model (solid line) semivariogram along the vertical direction for the various hydrofacies in the three zones. Notice that the range in the y-axis differs for gravel lithology.

Figure 7 Experimental (circle symbol) and model (solid line) semivariogram along the dip direction for the various hydrofacies in Zone 2 and Zone 3. Notice that the range in the y-axis differs for gravel lithology.

Figure 8 Experimental (circle symbol) and model (solid line) composited semivariogram along the vertical direction for the three zones.

Figure 9 Distribution of hydrofacies (after Zhu et al., 2015a) and $\log_{10}(K)$ in the three-dimensional domain representing the Chaobai alluvial fan: (a) axonometric projection of the three-dimensional system and (b) vertical sections along the A-A', B-B', C-C' and D-D' alignments. The vertical exaggeration is 25. The selected cell size is 300 m in north-south and east-west directions and 5 m in vertical direction, with a total number of 747, 540 cells. The thickness of the simulated domain is 300 m.

Figure 1

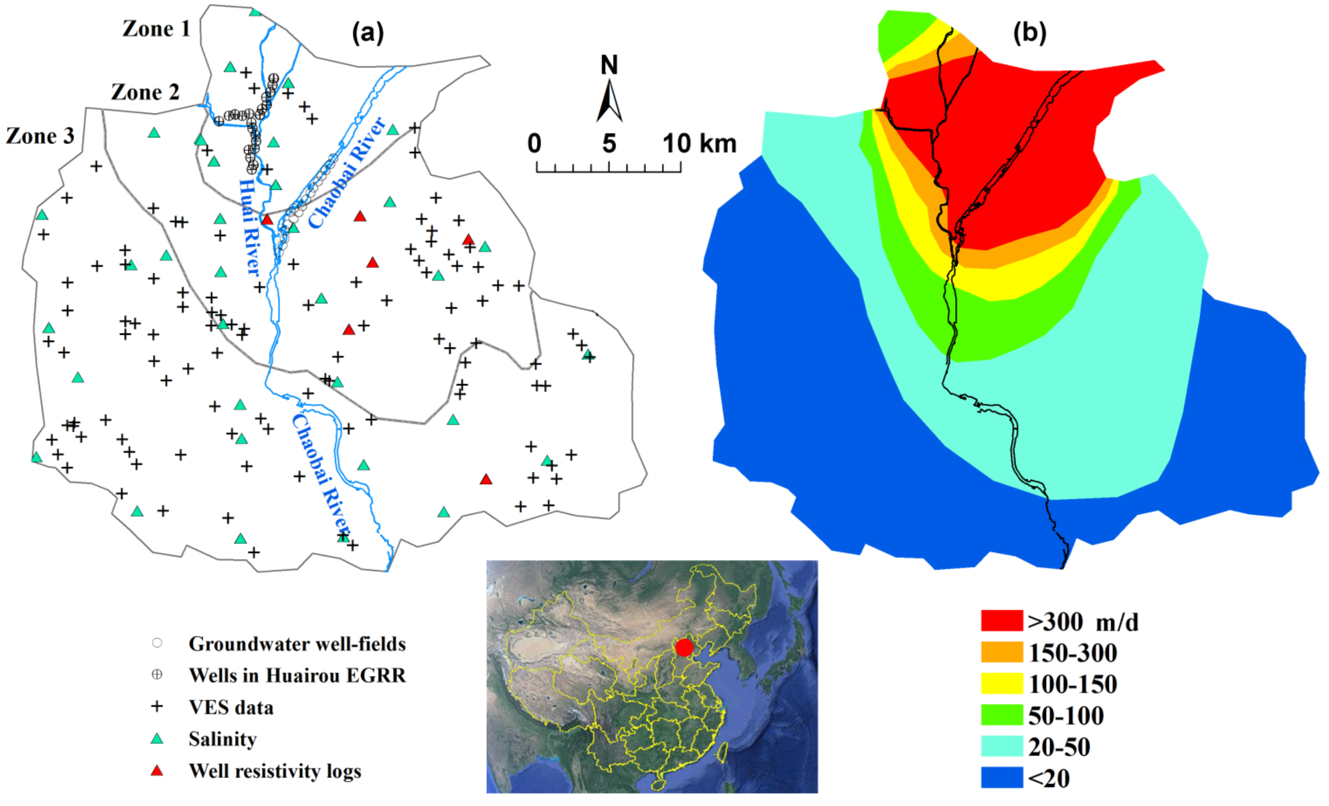
Zone 1
Zone 2
Zone 3
(a)
Huai River
Chaobai River
Chaobai River
N
0 5 10 km
(b)
Groundwater well-fields
Wells in Huairou EGRR
VES data
Salinity
Well resistivity logs
>300 m/d
150-300
100-150
50-100
20-50
<20

Figure 2

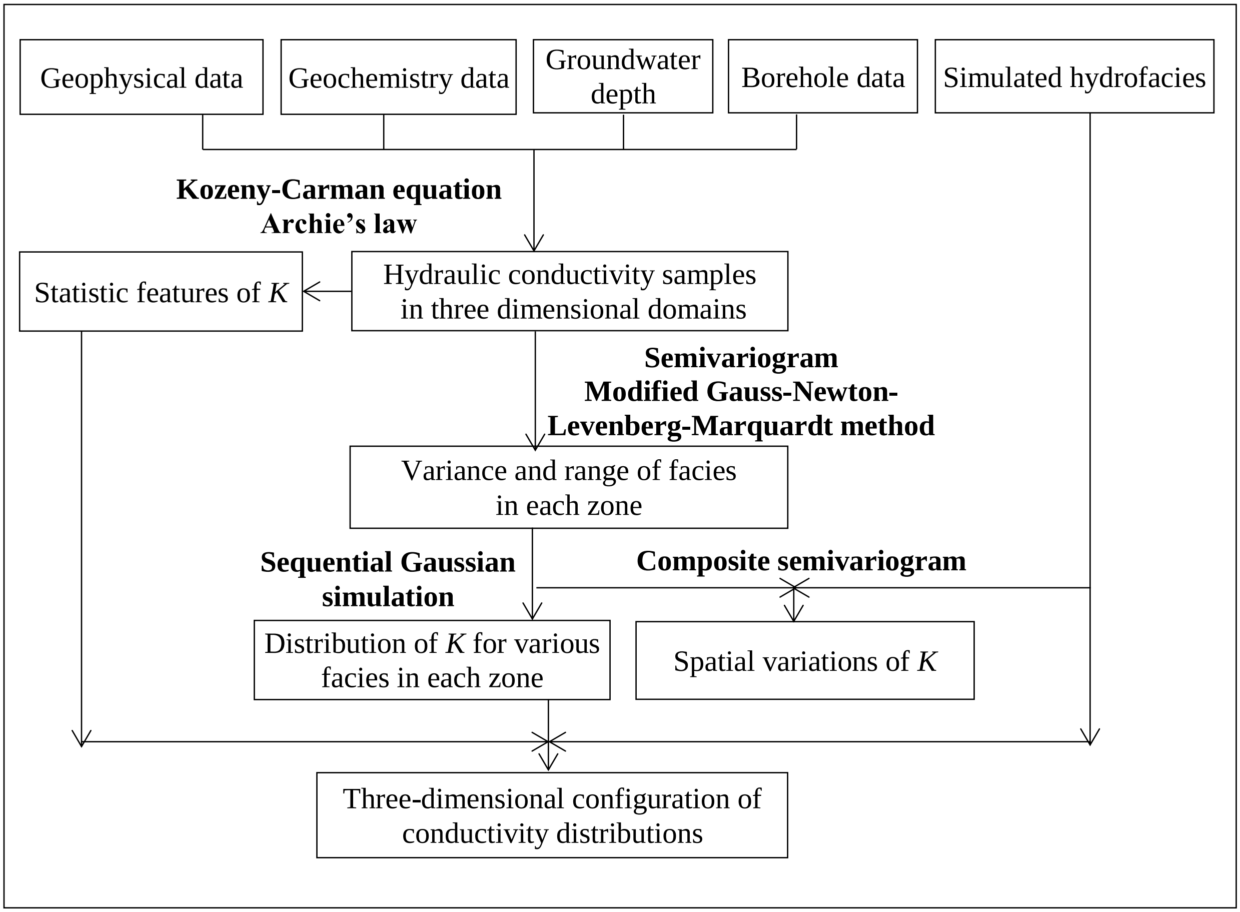

Geophysical data
Geochemistry data
Groundwater depth
Borehole data
Simulated hydrofacies
Kozeny-Carman equation
Archie's law
Statistic features of K
Hydraulic conductivity samples in three dimensional domains
Semivariogram
Modified Gauss-Newton-
Levenberg-Marquardt method
Variance and range of facies in each zone
Sequential Gaussian simulation
Composite semivariogram
Distribution of K for various facies in each zone
Spatial variations of K
Three-dimensional configuration of conductivity distributions

Figure3

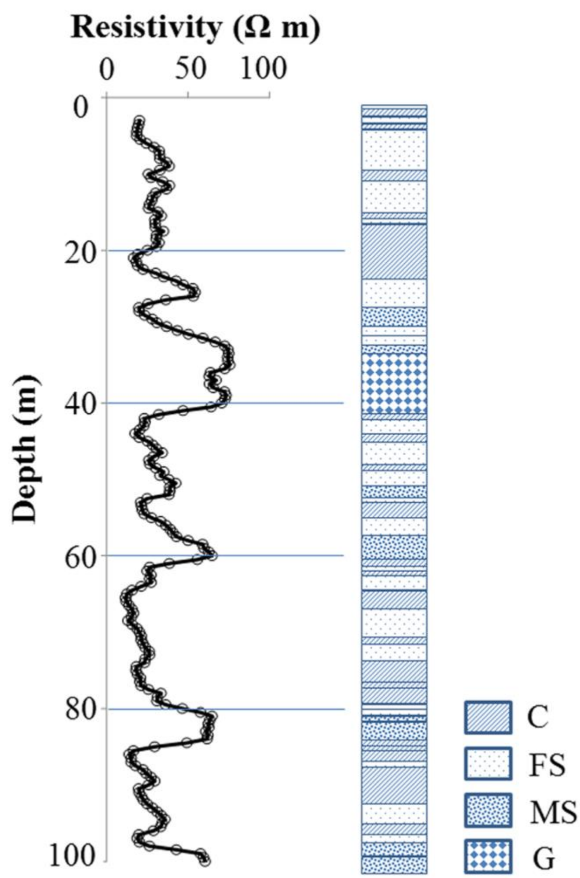

Figure 4

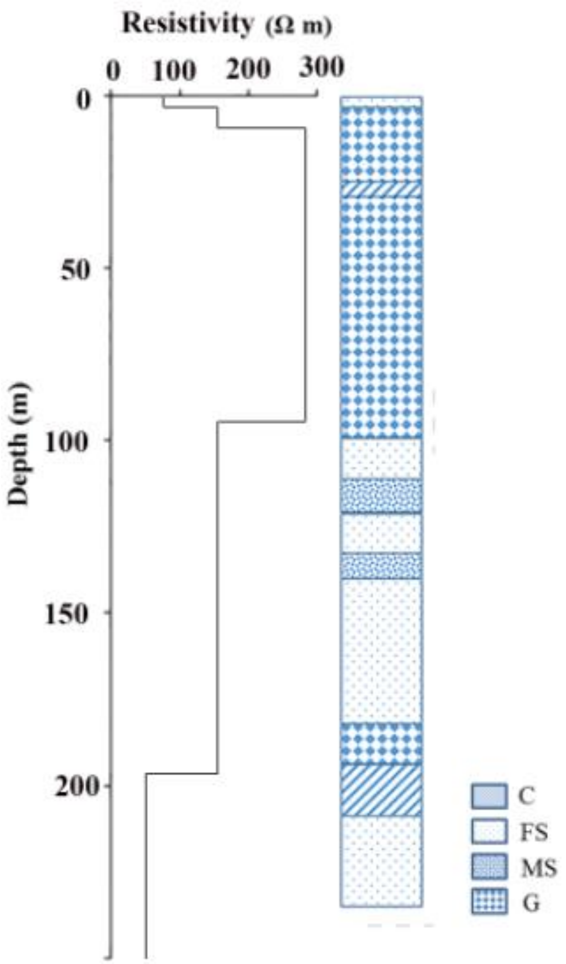

Figure 5

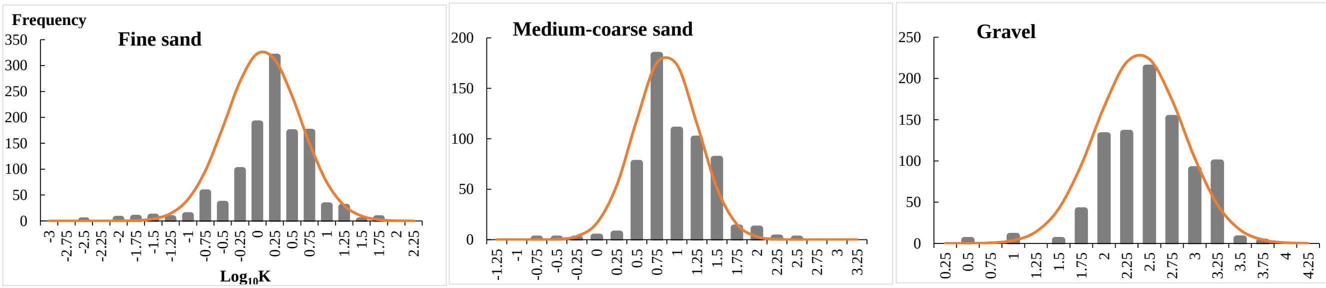

Figure 6

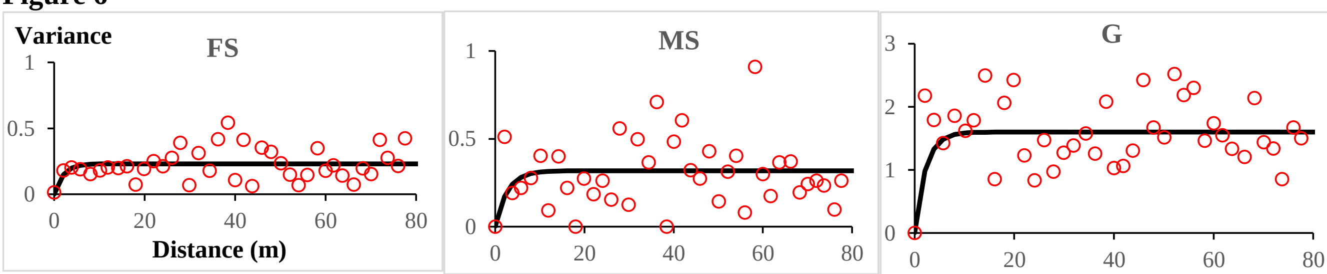

Zone1

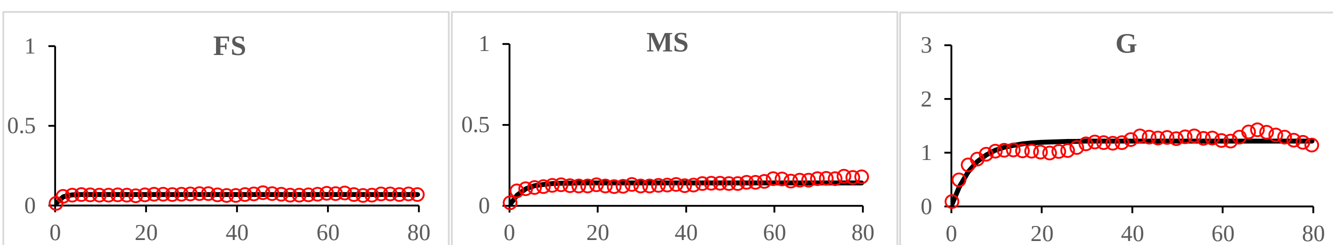

Zone 2

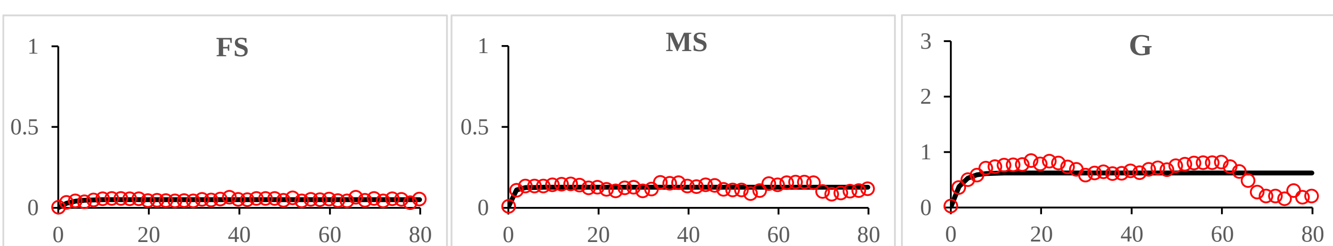

Zone 3

Figure 7

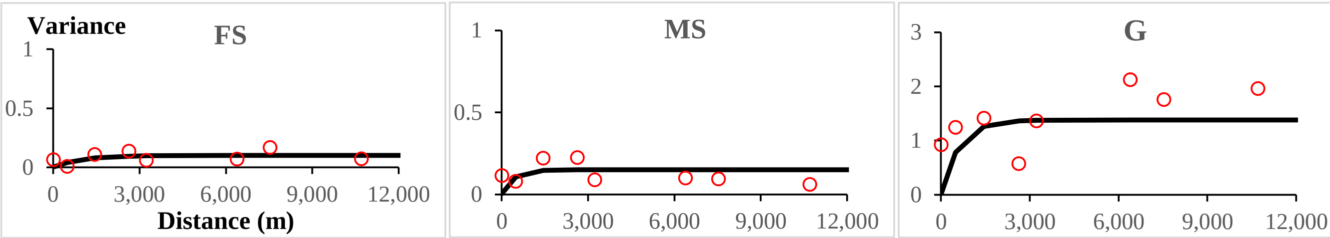

Zone 2

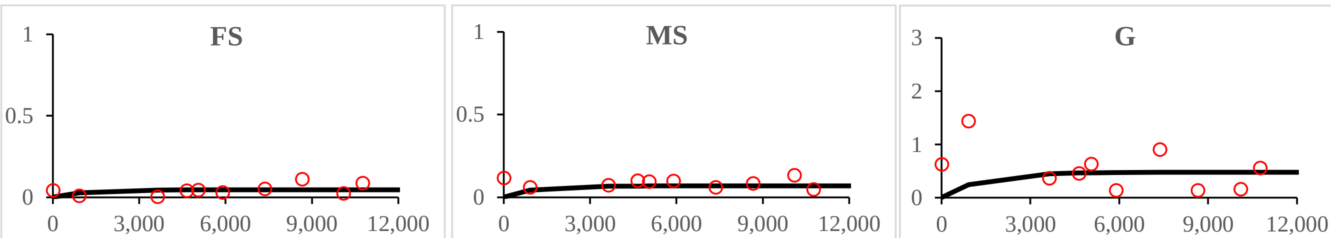

Zone 3

Figure 8

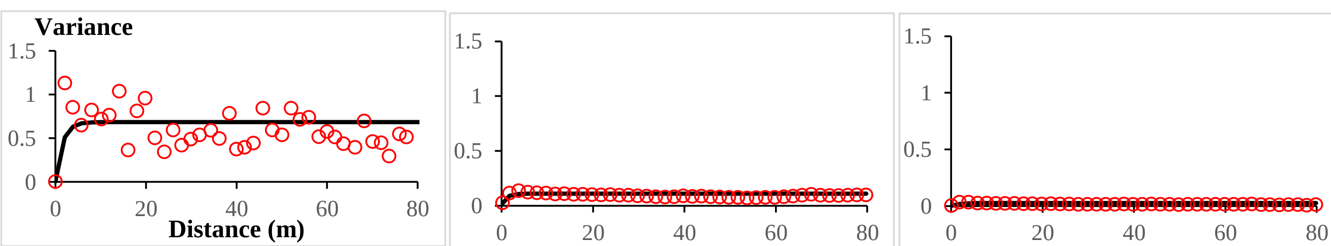

Zone 1 Zone 2 Zone 3

Figure 9

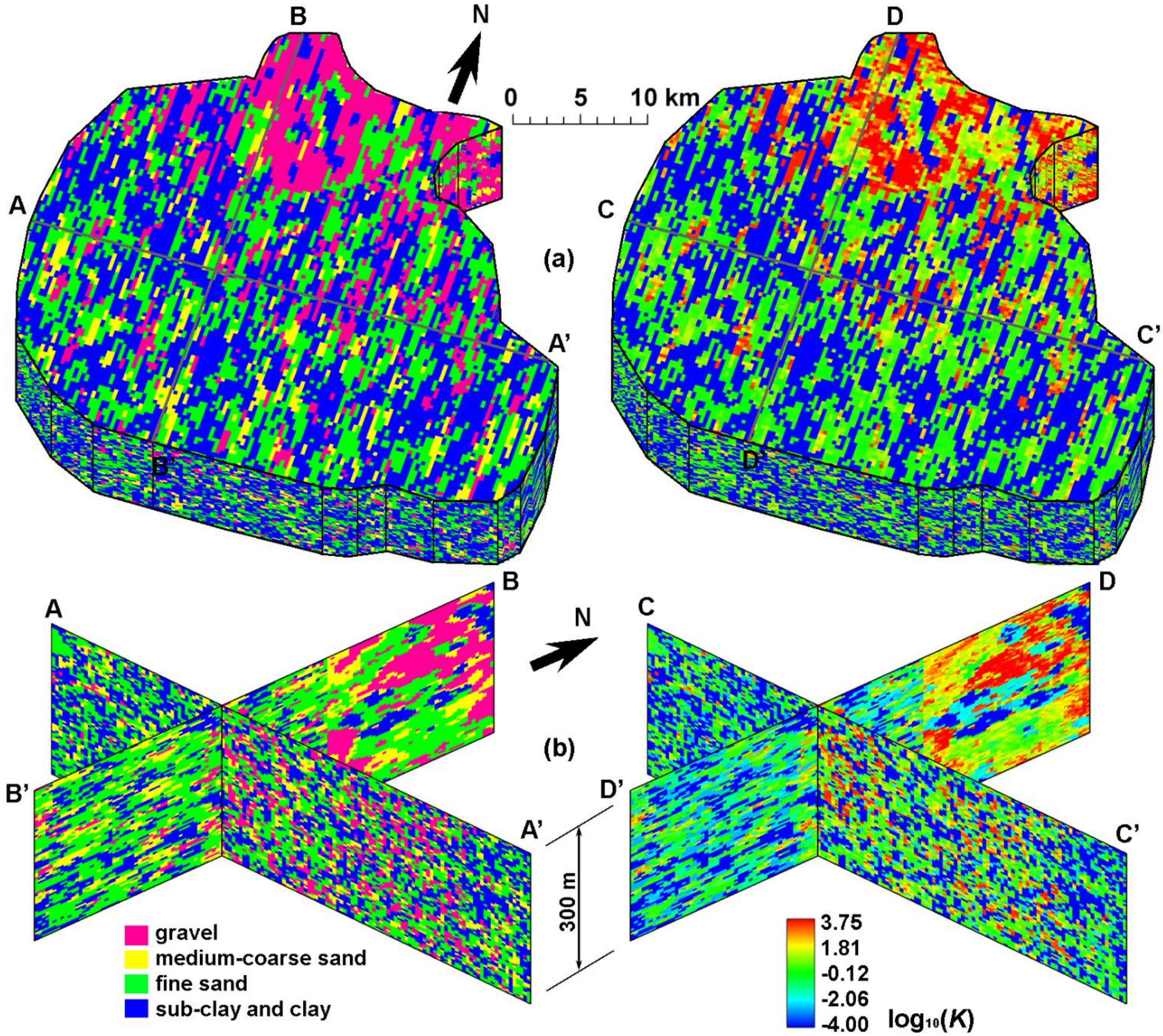
B
N
0
5
10 km
D
A
C
(a)
A'
C'
B'
D'
B
D
A
N
C
(b)
B'
D'
A'
C'
300 m
gravel
medium-coarse sand
fine sand
sub-clay and clay
3.75
1.81
-0.12
-2.06
-4.00
log10(K)